



Contents lists available at ScienceDirect

Tetrahedron

journal homepage: [www.elsevier.com/locate/tet](http://www.elsevier.com/locate/tet)

## Synthesis of novel 2*H*-indazole analogues *via* the Davis-Beirut reaction and conjugation onto magnetic nanoparticles

Mohammad H. El-Dakdouki <sup>a,\*</sup>, AbdulSattar Hussein <sup>a</sup>, Hiba Abdallah <sup>a</sup>, Rania Shatila <sup>b</sup>, Youssef Mouneimne <sup>b</sup>

<sup>a</sup> Department of Chemistry, Beirut Arab University, P.O. Box 11-5020, Riad El Solh, 11072809, Beirut, Lebanon

<sup>b</sup> KAS CRSL, American University of Beirut, Beirut, Lebanon

### ARTICLE INFO

#### Article history:

Received 5 May 2017

Received in revised form

4 August 2017

Accepted 14 August 2017

Available online xxx

#### Keywords:

2*H*-indazoles

Davis-Beirut reaction

Iron oxide nanoparticles

*In silico* toxicity

Hyaluronic acid

### ABSTRACT

Methods for the construction of C3-amino substituted 2*H*-indazole motifs are scarce. While the Davis-Beirut reaction proved useful and versatile in the construction of alkoxy- and thia- C3-substituted 2*H*-indazoles under mild basic conditions, the same success was not enjoyed when confronted with nitrogen-based nucleophiles. Therefore, we set out to expand the scope of the Davis-Beirut reaction and investigated the ability of amine nucleophiles to prompt the heterocyclization. In addition, a model 2*H*-indazole analogue was successfully conjugated onto magnetic nanoparticles for the first time. The toxicity of the synthesized analogues was estimated using *in silico* T.E.S.T software. This report provides a reliable approach for the synthesis of indazole-loaded nanoparticles whose applications have not been investigated before.

© 2017 Elsevier Ltd. All rights reserved.

### 1. Introduction

The indazole scaffold has recently received considerable attention due to its broad spectrum of biological activity that includes anticancer, anti-inflammatory, antidepressant, anti-HIV, and contraceptive activities.<sup>1</sup> Therefore, there is enormous potential in the synthesis of novel indazole motifs to be used as building blocks for the next generation of pharmaceuticals.<sup>2</sup> Naturally occurring indazoles are rare probably due to the difficulty of living organisms to construct N–N bonds.<sup>3,4</sup> This has enticed organic chemists to develop new facile synthetic routes to access the indazole core and optimize reported methods. While numerous synthetic approaches were reported for the preparation of the 1*H*-indazole tautomer, we are aware of only a handful of studies that have addressed the synthesis of substituted-2*H*-indazoles derivatives. As depicted in Scheme 1, routes to 2*H*-indazoles include DDQ oxidation of the corresponding pyrazoles made from the Bayllis-Hillman adducts of 2-cyclohexen-1-one (Scheme 1A),<sup>5</sup> copper-catalyzed intramolecular amination (Scheme 1B),<sup>6</sup> [3 + 2] dipolar cycloaddition of sydnone and arynes (Scheme 1C),<sup>7</sup> the indium-iodine reductive

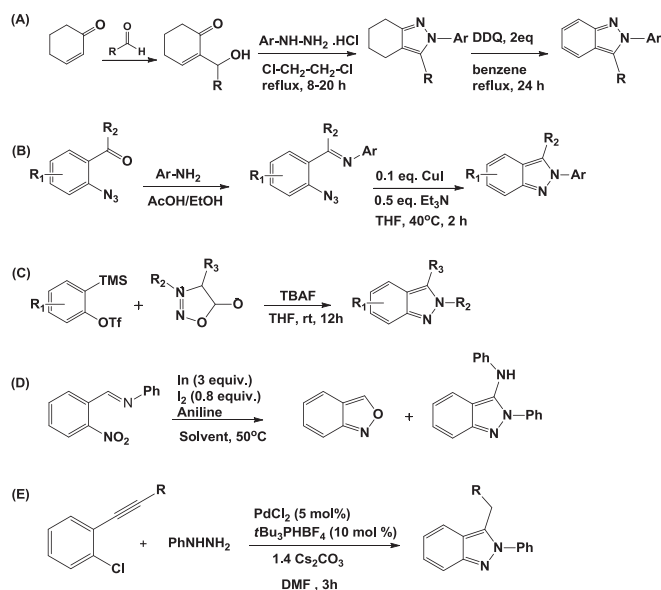
cyclization of 2-nitroaryl imine or 2-nitroarene precursors (Scheme 1D),<sup>8</sup> and the Pd-catalyzed intramolecular carbon–nitrogen bond formation (Scheme 1E).<sup>9</sup> Recently, inorganic nanoparticles such as copper (I) oxide<sup>10</sup> and copper (II) oxide<sup>11</sup> nanoparticles were employed to catalyze the formation of 2*H*-indazoles. Despite the achieved success, most of these methods still have limitations, and new routes are still explored.

Most recently, the Davis-Beirut reaction has been introduced as a simple, efficient, and versatile base-mediated *N,N*-bond forming heterocyclization one-pot reaction for the preparation of a wide variety of all-new 2*H*-indazoles and indazolones.<sup>12–15</sup> The named reaction led to the successful preparation of 3-alkoxy,<sup>13</sup> 3-thia,<sup>16</sup> and 3-amino substituted 2*H*-indazoles which are the focus of this study (Scheme 2).<sup>17</sup> Substrate diversity in the Davis-Beirut reaction presents itself in the numerous heterocycles that can easily be fused to the 2*H*-indazole core. Such heterocycles would be difficult to prepare by other methods.

Unfortunately, the success and versatility achieved in the preparation of alkoxy- and thia-based 2*H*-indazoles under the Davis-Beirut reaction conditions was not attained in the synthesis of amino-based 2*H*-indazoles (i.e. using an alkylamine as the nucleophile) which proved to be tedious. In this regard, only one report described the synthesis of C3-amino-substituted-2*H*-indazoles using aminobenzothiazole as the nucleophile and 1,8-

\* Corresponding author.

E-mail address: [m.eldakdouki@bau.edu.lb](mailto:m.eldakdouki@bau.edu.lb) (M.H. El-Dakdouki).



Scheme 1. Routes to 2H-indazole.

diazabicyclo[5.4.0]undec-7-ene (DBU) as a base.<sup>17</sup> Thus, much work is needed to extend the scope of the Davis-Beirut reaction.

Nanotechnology has emerged as a promising tool that has found numerous applications in the medical field for the detection, diagnosis, and treatment of diseases.<sup>18</sup> While the indazole pharmacophore has been investigated for diverse biological and industrial applications, no report has described the conjugation of indazoles onto nanoparticles. Iron oxide nanoparticles have long been used in diverse medical applications including drug delivery and disease detection.<sup>19,20</sup> It is crucial that the nanoparticles are biocompatible and colloidally stable if they are to be administered systemically in living organisms.<sup>21</sup> In this regard, dextran-coated superparamagnetic iron oxide nanoparticles (SPIONs) have been used in biological systems.<sup>22</sup> Two SPIONs agents, namely Feridex and Resovist, are approved for clinical application.<sup>23</sup> Hence, SPIONs were selected as an ideal system to act as a carrier of the synthesized 2H-indazole analogues. As the ultimate goal, which is beyond the scope of this study, is to assess the biological activity of the indazole-loaded nanoparticles in biological systems, we relied on an *in silico* computer-based predictive model to estimate the potential toxicity of the synthesized indazole analogues, and to direct the future synthesis of biologically compatible molecules. Therefore, in this study, we aim at: (i) Optimizing the Davis-Beirut reaction conditions to yield the desired C3-amino substituted indazoles analogues in good yields. Achieving this goal aims towards avoiding the low synthetic productivity of the Davis-Beirut reaction when confronted with nitrogen-based nucleophiles; (ii)

Synthesizing and characterizing the indazole-loaded magnetic nanoparticles. This goal will be achieved by preparing hyaluronan-coated superparamagnetic iron oxide nanoparticles, and the subsequent conjugation of the 2H-indazole analogues *via* amide bond formation; and (iii) Estimating the toxicity of the synthesized 2H-indazoles *in silico*.

## 2. Results and discussion

### 2.1. Synthesis of benzylamine amine derivatives

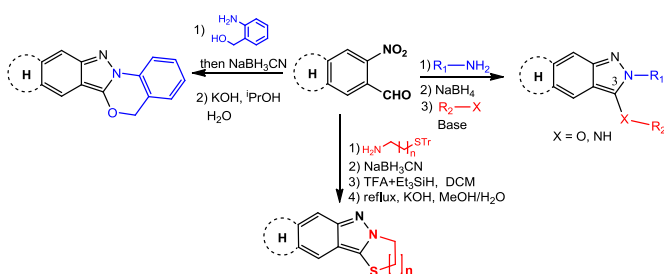
The benzylamine derivatives **3** which act as the synthetic precursors for the desired 2H-indazoles were prepared as depicted in Scheme 3. First, the Schiff bases were synthesized in excellent yields by melting 6-methoxy-benzothiazol-2-ylamine **1** with the corresponding *o*-nitrobenzaldehyde derivative **2** at 120 °C.<sup>17</sup> The as-prepared Schiff bases were then reduced to the corresponding benzylamine derivatives **3** using sodium borohydride as reducing agent. The reaction was complete when all orange Schiff bases were converted into yellow benzylamine precipitate. The reduction was highly efficient and the benzylamines required no further purification as revealed by various spectroscopic techniques (Supporting information).<sup>17</sup>

### 2.2. Synthesis of the 2H-indazole analogues via the Davis-Beirut reaction

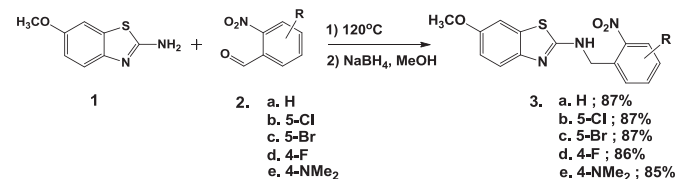
As our goal is to conjugate 2H-indazole analogues onto the surface of iron oxide nanoparticles, we set out to synthesize indazole derivatives equipped with a linker at the C-3 position bearing a primary amino group to facilitate its linkage to carboxyl-functionalized nanoparticles. We opted to access the target 2H-indazole analogues **4** from the corresponding benzylamines *via* the Davis-Beirut reaction using DBU as the base at room temperature as depicted in Scheme 4.

As amine nucleophiles did not enjoy the same success as the alkoxy- and thia-based counterparts, the reaction conditions were optimized to yield the desired indazoles in good yields. We first attempted to synthesize the indazole analogues with ethylene diamine (EDA, **7a**) at the C-3 position of the indazole ring. Monitoring the conversion of benzylamine **3a** by MS confirmed the formation of the desired product **5** (Fig. S38). Unfortunately, compound **5** was obtained in very low yield (<5%) and its purification by column chromatography or thick layer chromatography proved to be tedious. Similar results were obtained when triethylene glycol diamine (NH<sub>2</sub>-TEG-NH<sub>2</sub>) **7b** was used as a linker (Fig. 1). Isolation and analysis of an analytical sample by proton NMR spectroscopy and MS confirmed the structure of the desired indazoles **6a** and **6d** (Fig. 1, Fig. S39 and S40). However, the low yield of reactions (<5%) hindered the applicability of the deployed approach.

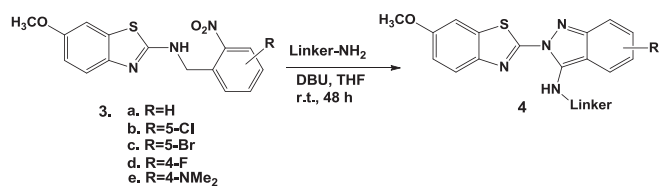
To overcome this synthetic hurdle, we postulated that protecting one of the primary amino groups of the diamine linkers **7a** and **7b** with a base-resistant protecting group such as *tert*-butyloxycarbonyl group (Boc), might afford the desired indazole analogues in acceptable yields. Thus, the Boc-protected linkers namely Boc-



Scheme 2. Synthetic versatility of the Davis-Beirut reaction.



Scheme 3. Synthesis of the benzylamine derivatives.



**Scheme 4.** Synthesis of 2*H*-indazole derivatives via the Davis-Beirut reaction.

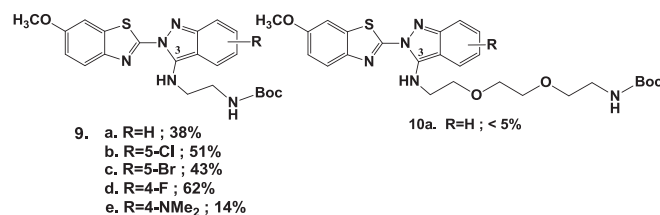


**Fig. 2.** Structures of Boc-protected 2*H*-indazoles.

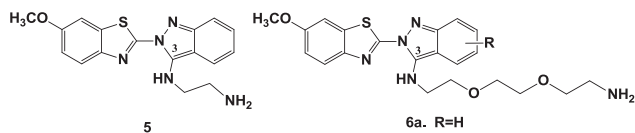
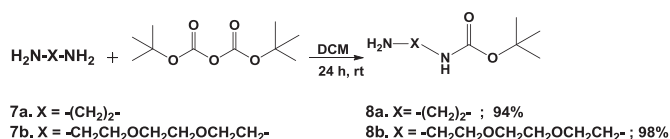


**Fig. 1.** Structures of 2*H*-indazoles **5**, **6a** and **6d** prepared under Davis-Beirut reaction conditions with deployed linkers.

EDA-NH<sub>2</sub> **8a** and Boc-TEG-NH<sub>2</sub> **8b** were prepared in excellent yields by dropwise addition of Boc anhydride (Boc<sub>2</sub>O) solution in anhydrous DCM to five equivalents of the corresponding diamine (Scheme 5).<sup>24</sup>

When benzylamine **3a** and Boc-TEG-NH<sub>2</sub> **8b** were reacted under the Davis-Beirut reaction conditions, indazole **10a** was obtained as confirmed by MS (Fig. S47), but only in low yields (Fig. 2). Interestingly, indazole **9a** with Boc-EDA linker at C-3 was afforded in good yield as confirmed by NMR spectroscopy and MS (Figs. S48–S51). The poor outcome of the reaction with Boc-TEG compared to that of Boc-EDA-NH<sub>2</sub> can be rationalized by the reduced nucleophilicity of the amino group due to the presence of a nearby electron withdrawing oxygen. Thus, Boc-EDA was the linker of choice for the synthesis of the proposed 2*H*-indazole derivatives **9a–e** (Fig. 2). The successful synthesis of 2*H*-indazole derivatives was confirmed by various spectroscopic techniques. The <sup>1</sup>H NMR spectroscopy revealed the disappearance of the peak around 5 ppm of the benzylic methylene group of the benzylamine derivative, the presence of eight to ten aromatic hydrogen atoms depending on the degree of ring substitution, the presence of a sharp singlet around 1 ppm that counted for the nine hydrogens of the Boc moiety, and the presence of two peaks at 3.5 and 3.9 ppm that integrated for two protons each and accounted for the ethylene group in the linker. Results were further confirmed by <sup>13</sup>C NMR spectroscopy that showed peaks around 27 and 28 ppm assigned to the methylene carbons in the linker. Further evidence was collected by MS (Supporting information).

As expected, the yield of the Davis-Beirut reactions appeared to be influenced by the electronic properties of the substituent on the benzene ring. While benzylamine derivatives with electron withdrawing groups such as fluorine in **3d**, chlorine in **3b**, and bromine in **3c** afforded the highest yields for indazoles **9d** (62%), **9b** (51%), and **9c** (42%), those with electron donating groups such as dimethylamino in **3e** produced the desired indazole **9e** only in 14% yield. It seems that presence of an electron-withdrawing group enhances the electrophilicity of the nitro group rendering it more susceptible to deoxygenation or reduction, forming the nitroso aldehyde



**Scheme 5.** Synthesis of Boc-protected linkers.

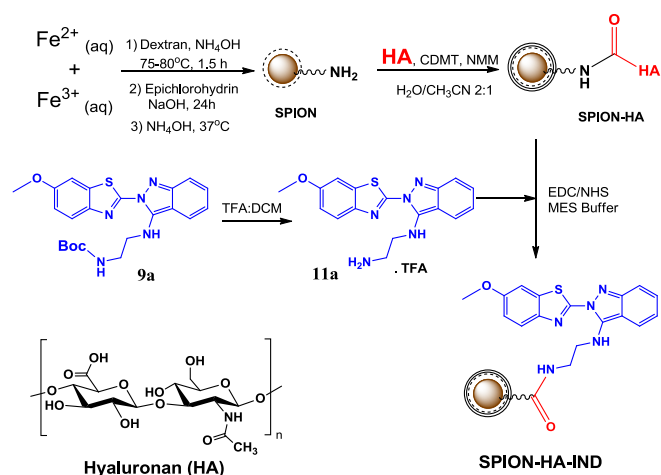
intermediate.<sup>17</sup> On the other hand, an electron-donating group has the opposite effect. Furthermore, the optimal reaction conditions were found to be stirring the reaction mixture at room temperature for 48 h. Longer reaction times did not result in better yields, while heating the reaction mixture adversely affected the outcome especially under reflux conditions.

### 2.3. Synthesis of indazole-loaded nanoparticles

With their nanometer dimensions and unique magnetic properties, iron oxide nanoparticles have been used in a variety of biological applications including bioseparation, biosensing, noninvasive imaging, targeted drug delivery as well as disease treatment based on hyperthermia.<sup>20</sup> Dextran-coated superparamagnetic iron oxide nanoparticles (SPIONs) have been selected as the carrier of the synthesized 2*H*-indazole analogues due to its biocompatibility and colloidal stability. The dextran-coated SPIONs were synthesized following the coprecipitation method.<sup>25,26</sup> In brief, an aqueous solution of ferric and ferrous ions was neutralized by ammonium hydroxide in the presence of dextran at 80 °C, followed by crosslinking the dextran with epichlorohydrin to induce stability to the surface coating. Amino groups were introduced into the surface by stirring the crosslinked nanoparticles in an ammonium hydroxide solution for 2 days at 37 °C (Scheme 6). It is desirable that the surface of the nanoparticles is functionalized with carboxyl groups to ensure that the 2*H*-indazole derivatives with free primary amine groups can be conjugated through amide bonds. To achieve this goal, the biocompatible hyaluronic acid (HA) was selected as the polymer of choice.<sup>27</sup> HA coating provides stability against agglomeration and opsonization. It also provides the necessary carboxyl groups which serve as chemical handles for the conjugation of the synthesized analogues onto the nanoparticles by amidation. A sonicated aqueous solution of hyaluronic acid was activated with 2-chloro-4,6-dimethoxy-1,3,5-triazine (CDMT) and *N*-methylmorpholine (NMM) and the reaction was allowed to stir at room temperature for 2 h after which the aqueous dispersion of SPION was added and the mixture was stirred for 48 h to provide SPION-HA (Scheme 6).

SPION-HA exhibited a hydrodynamic diameter of 88 nm as measured by Dynamic Light Scattering (DLS) (Fig. 3A), and an iron oxide core of 5–7 nm in diameter as revealed by TEM (Fig. S62). A polydispersity index of 0.24 confirmed the monodispersity of SPION-HA. Thermal gravimetric analysis (TGA) provided evidence for the successful conjugation of HA onto SPION and demonstrated that HA accounted for 44% weight of each SPION-HA (Fig. 3C). The potential use of SPION-HA nanoparticles as negative MRI contrast agents was assessed by measuring its ability to enhance the T<sub>2</sub>\* magnetic relaxation rate ( $r_2^* = 1/T_2^*$ ) of water in a magnetic field. SPION-HA had excellent magnetic relaxivity ( $r_2^* = 232 \text{ mM}^{-1} \text{ s}^{-1}$  at 3T), thus are good contrast agents for T<sub>2</sub>\* weighted MRI (Fig. 3D).

The 2*H*-indazole analogues were then conjugated to SPION-HA, with indazole **9a** chosen as the model molecule to run preliminary experiments. To facilitate the conjugation of indazole **9a** onto the HA-coated nanoparticles via an amide bond, the Boc protecting



**Scheme 6.** Preparation of indazole-loaded magnetic nanoparticles.

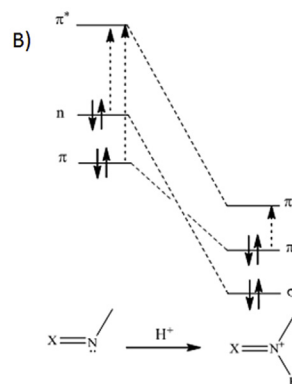
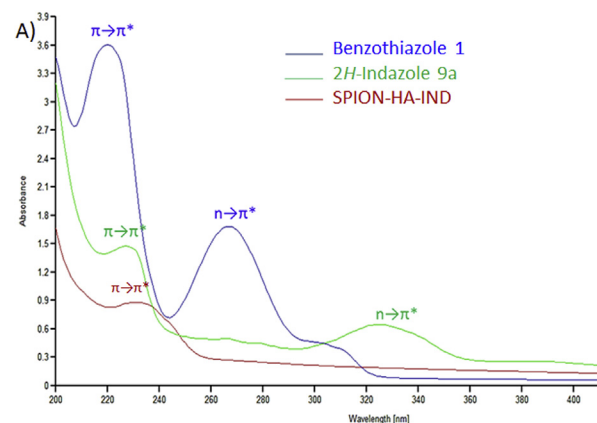
group was removed under acidic conditions to yield the indazole **11a** with a free amino group (Scheme 6). HA was activated using EDC/NHS coupling chemistry in MES buffer. Indazole **11a** in MES:DMSO was then added, and the reaction was allowed to stir in the dark over 48 h to provide the SPION-HA-IND that was purified by centrifugation.

The loading of analogue **11a** onto the surface of the nanoparticles was revealed by UV–vis spectroscopy. The absorbance pattern of indazole-loaded nanoparticle SPION-HA-IND was compared to that of 6-benzothiazolamine **1** and the indazole **9a** (Fig. 4A). Precursor **1** showed an absorbance maximum at 220 assigned to  $\pi \rightarrow \pi^*$  transition (benzene ring) and another band at 265 nm ( $n \rightarrow \pi^*$ ). The 2*H*-indazole **9a** showed a red shift to 230 nm (aromatic ring) due to lengthening of a  $\pi$ -conjugated system, and a band at 326 nm attributed to  $n \rightarrow \pi^*$  transition. The successful conjugation of the indazole onto SPION-HA was inferred *via* absorbance at 230 nm ( $\pi \rightarrow \pi^*$ ). Interestingly, the absorption band at 326 nm ( $n \rightarrow \pi^*$ ) disappeared. This has been attributed to the possible protonation of the lone pair (n) of electrons on nitrogen under the acidic coupling reaction conditions. As a result, the lone pair (n) becomes a bonding pair ( $\sigma$ ). Furthermore, all electrons are now held more tightly and all MO energy levels are lowered

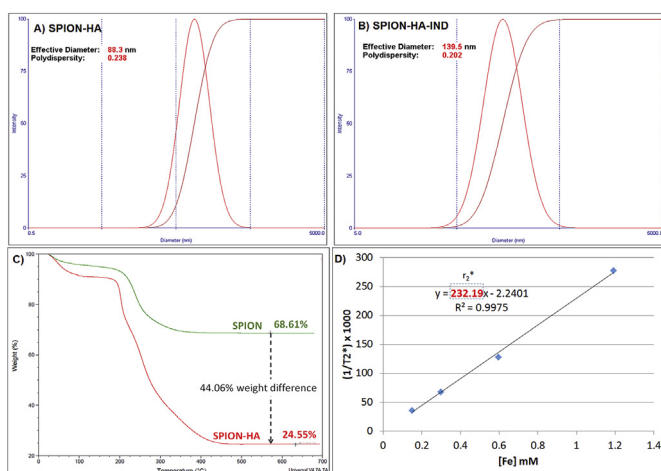
especially the LUMO (Fig. 4B). The concentration of the indazole loaded onto the nanoparticles was 0.071 mg/ml. Further evidence was obtained by comparing the difference in the effective hydrodynamic diameters of the nanoparticles. While the hydrodynamic diameter of SPION-HA was measured to be 88 nm, the conjugation of the 2*H*-indazole **11a** onto the nanoparticles resulted in an increase in the size of the nanoparticles yielding SPION-HA-IND with diameter of 139 nm (Fig. 3B). The polydispersity index of the SPION-HA-IND was found to be 0.2, highlighting the monodispersity of the nanoparticles and reflecting its potential safe application in biological systems (Fig. 3B).

#### 2.4. *In silico* toxicity prediction for the synthesized 2*H*-indazole analogues

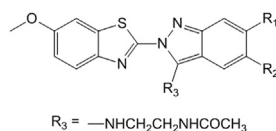
As the synthesized 2*H*-indazole analogues (free and conjugated onto nanoparticles) are to be evaluated for diverse biological activities in living organisms, we set out to assess its potential toxicity using the Toxicity Estimation Software Tool (T.E.S.T.; version 4.2.1).<sup>28</sup> T.E.S.T. is an *in silico* computer-based predictive model developed by the USA Environmental Protection Agency (EPA) to screen untested compounds in order to establish priorities for expensive and time-consuming traditional bioassays designed to establish toxicity levels. The consensus method was used to assess developmental toxicity, rat lethal dose (LD<sub>50</sub>), and Ames mutagenicity. Developmental toxicity predicts whether a chemical interferes with normal development of humans and animals both before and after birth. A compound is classified Ames positive if it significantly induces revertant colony growth in at least one of out of five strains. The oral rat LD<sub>50</sub> endpoint represents the amount of the chemical (mass of the chemical per body weight of the rat)



**Fig. 4.** (A) UV–vis spectra of benzothiazole **1**, 2*H*-indazole **9a**, and SPION-HA-IND. (B) Spectral red shift of  $\pi \rightarrow \pi^*$  transition upon protonation.



**Fig. 3.** Hydrodynamic diameter of SPION-HA (A) and SPION-HA-IND (B). (C) Thermogravimetric analysis of SPION and SPION-HA showing 44% weight difference in organic coating resulting from the successful conjugation of HA onto the nanoparticles. (D) Determination of magnetic relaxivity ( $r_2^* = 232 \text{ mM}^{-1} \text{ s}^{-1}$ ) of SPION-HA.

**Table 1***In silico* toxicity prediction for some 2*H*-indazole analogues.

Entry	R <sub>1</sub>	R <sub>2</sub>	Oral Rat LD <sub>50</sub> (mg/kg)	Mutagenicity <sup>a</sup> (a.u.)	Developmental Toxicity <sup>b</sup> (a.u.)
1	H	H	1047.50	0.79 (Positive)	0.48 (Non-toxicant)
2	F	H	1561.09	0.85 (Positive)	0.60 (Toxicant)
3	H	Cl	633.56	0.84 (Positive)	0.54 (Toxicant)
4	H	Br	1921.91	0.75 (Positive)	0.82 (Toxicant)
5	N(CH <sub>3</sub> ) <sub>2</sub>	H	764.03	0.58 (Positive)	0.55 (Toxicant)
6	H	CH <sub>3</sub>	1616.70	0.94 (Positive)	0.31 (Non-toxicant)
7	CH <sub>3</sub>	H	1250.98	0.70 (Positive)	0.31 (Non-toxicant)
8	C(CH <sub>3</sub> ) <sub>3</sub>	h	1487.11	0.47 (Negative)	0.32 (Non-toxicant)

<sup>a</sup> Chemicals with predicted value > 0.5 are considered mutagenicity positive.<sup>b</sup> Chemicals with predicted value > 0.5 are considered toxicants.

which when orally ingested kills half of the sample rats.

The toxicity parameters were assessed for the acetamide analogues of the 2*H*-indazoles to mimic the amide linkage between hyaluronic acid on the nanoparticles and the synthesized indazoles. The *in silico* toxicity predictions are summarized in Table 1. Only the unsubstituted 2*H*-indazole (entry 1) was predicted not to exhibit developmental toxicity, and all synthesized analogues (entries 1–5) were predicted to induce mutagenicity. The predicted oral rat LD<sub>50</sub> values for the prepared analogues (entries 1–5) ranged from 633.56 mg/kg for the 5-chloro-substituted analogue to 1921.91 mg/kg for the 5-bromo-substituted analogue, indicating that the former is the most toxic while the latter is the least. To set the stage for future design and synthesis of novel non-toxic 2*H*-indazole analogues, we estimated the toxicity of several analogues. The software predicted that the presence of an electron donating group such a methyl (entries 6–7) lowered developmental toxicity but not mutagenicity. Interestingly, the presence of a bulky *tert*-butyl group (entry 8) yielded an analogue that is neither a developmental toxicant nor mutagenic.

### 3. Conclusion

The novelty of the current study stems not only from the preparation of novel heterocyclic 2*H*-indazoles compounds *via* the Davis-Beirut reaction, but also from extending the scope of the named reaction by overcoming a major limitation represented in the introduction of an amine substituent on position C-3 of the heterocycle. The reactions were conducted under mild conditions without the need of special reagents or catalysts. In addition, the successful conjugation of a model 2*H*-indazole analogue onto magnetic nanoparticles has not been reported before. The *in silico* toxicity predictions provide a tool for designing future potentially safe 2*H*-indazoles analogues. The synthetic accessibility and feasibility of indazole-loaded nanoparticles opens new avenues for assessing the previously unexplored biomedical applications of this novel formulation.

### 4. Experimental section

Reagents were purchased from local suppliers and used without further purification. *o*-nitrobenzaldehyde, 4-dimethylamino-2-nitrobenzaldehyde, 4-fluoro-2-nitrobenz-aldehyde, 4-bromo-2-nitrobenzaldehyde, methanol, sodium borohydride, trifluoroacetic acid, ethylene diamine, and diaminated triethylene glycol, ferric

chloride hexahydrate (FeCl<sub>3</sub>·6H<sub>2</sub>O), NH<sub>4</sub>OH (36%), ferrous chloride tetrahydrate (FeCl<sub>2</sub>·4H<sub>2</sub>O), and dextran (13–20 kDa) were obtained from Sigma-Aldrich. 6-methoxy-benzothiazol-2-ylamine, 5-chloro-2-nitrobenzaldehyde, DBU, NMM, CDMT, anhydrous DCM, anhydrous methanol, and anhydrous THF were purchased from Across Organics. Di-*tert*-butyldicarbonate was obtained from Fluka. DCM reagent grade was attained from Fischer Scientific. Instrumental analysis was carried out at Beirut Arab University unless stated otherwise.

NMR data were recorded with a Bruker 300 MHz spectrometer and chemical shifts were reported as ppm downfield from TMS as internal standard. Melting points were recorded with Gallenkamp digital Melting-point apparatus and were not corrected. FTIR spectra was attained on a Nicolet Avatar 360 FT-IR spectrometer in KBr discs at the American University of Beirut. Dynamic Light Scattering (DLS) analysis was collected on a NanoBrook 90Plus particle size analyser in the Department of Chemical and Petroleum Engineering at the American University of Beirut. Mass spectroscopy spectra were obtained on the Waters Quattro micro API LC/MS/MS at Michigan State University (USA), or on AGILENT 1100 Series Quaternary Pump HPLC, with Agilent LC/MSD Trap XCP Mass Spectrometry Detector at the American University of Beirut Spectrophotometry was attained using a Jasco V-670 spectrophotometer. Concentration refers to rotary evaporation of volatiles. Thermogravimetric analysis (TGA) was carried on a Thermal Advantage (TA-Instruments-Waters LLC) TGA-Q500 series and the samples were burned under nitrogen. Relaxivity measurements were carried out on a GE 3T Signa<sup>®</sup> HDx MR scanner (GE Healthcare, Waukesha, WI) at Michigan State University (USA).

#### 4.1. Synthesis of Benzylidene amine derivatives

An equimolar mixture of 6-methoxy-benzothiazol-2-ylamine **1** and an *o*-nitrobenzaldehyde derivative **2** was melted in an oil bath set around 120 °C to ensure complete melting and removal of water as it forms. The reaction proceeded until TLC showed consumption of the starting materials. Purification as required is given for each synthesis.

##### 4.1.1. *N*-(6-methoxy-benzothiazol-2-yl)-2-nitrobenzylidene amine

(6-Methoxy-benzothiazol-2-yl)-amine **1** (0.54 g, 3 mmol) and *o*-nitrobenzaldehyde **2a** (0.5 g, 3 mmol) were used and the corresponding Schiff base was obtained as a yellow solid in 92% yield following purification on a silica gel column using DCM as an

eluent. M.p. 178–180 °C;  $^1\text{H}$  NMR (300 MHz, DMSO)  $\delta_{\text{H}}$  3.98 (s, 3H), 7.09 (dd,  $J = 6.12, 3.05$ , 1H), 7.30 (d,  $J = 6.24$ , 1H), 7.70–7.77 (m, 2H), 7.90 (d,  $J = 6.81$ , 1H), 8.11 (d,  $J = 6.34$ , 1H), 8.45 (d,  $J = 6.67$ , 1H), 9.49 (s, 1H);  $^{13}\text{C}$  NMR (100 MHz, DMSO)  $\delta_{\text{C}}$  55.81, 104.24, 116.13, 124.35, 124.85, 129.50, 130.05, 132.61, 133.96, 136.16, 146.05, 149.79, 158.15, 160.5, 168.01; IR (KBr)  $\nu_{\text{max}}$ : 755 (s), 1122 (m), 1530 (s), 1647 (m), 3411 (s); MS: Theoretical mass: 313.05 calculated for  $\text{C}_{15}\text{H}_{11}\text{N}_3\text{O}_3\text{S}$ ; Found:  $m/z$   $[\text{M}+\text{H}]^+$ : 314.06;

#### 4.1.2. *N*-(6-methoxy-benzothiazol-2-yl)-5-chloro-2-nitrobenzylidene amine

(6-Methoxy-benzothiazol-2-yl)-amine **1** (0.54 g, 3 mmol) and 5-chloro-*o*-nitrobenzaldehyde **2b** (0.55 g, 3 mmol) were used, and the corresponding Schiff base was obtained as a reddish solid 94% yield following purification by column chromatography using DCM as an eluent. M.p. 165–166 °C;  $^1\text{H}$  NMR (300 MHz, DMSO)  $\delta_{\text{H}}$  3.85 (s, 3H), 7.15 (dd,  $J = 6.97, 6.32$ , 1H), 7.80 (dd,  $J = 6.36, 5.72$ , 1H), 7.92–7.94 (m, 2H), 8.21–8.23 (m, 2H), 9.42 (s, 1H);  $^{13}\text{C}$  NMR (100 MHz, DMSO)  $\delta_{\text{C}}$  55.02, 105.08, 105.59, 116.32, 123.86, 126.46, 127.01, 129.01, 130.82, 132.64, 133.55, 135.97, 138.69, 145.41, 145.87, 147.24, 147.99, 154.81, 157.71, 161.19, 162.49, 167.37, 188.67; IR (KBr)  $\nu_{\text{max}}$ : 827 (s), 1225 (s), 1525 (s), 1605 (s), 2940 (w);

#### 4.1.3. *N*-(6-methoxy-benzothiazol-2-yl)-5-bromo-2-nitrobenzylidene amine

The product was obtained as reddish solid from (6-methoxy-benzothiazol-2-yl)-amine **1** (0.54 g, 3 mmol) and 5-bromo-*o*-nitrobenzaldehyde **2c** (0.69 g, 3 mmol) in 96% yield following recrystallization from DCM. M.p. 155–157 °C;  $^1\text{H}$  NMR (300 MHz, DMSO)  $\delta_{\text{H}}$  3.85 (s, 3H), 6.80 (dd,  $J = 8.73, 6.06$ , 2H), 7.23 (d,  $J = 8.79$ , 1H), 7.70 (d,  $J = 2.52$ , 1H), 7.90 (d,  $J = 8.94$ , 1H), 8.41 (d,  $J = 1.83$ , 1H), 9.37 (s, 1H);  $^{13}\text{C}$  NMR (100 MHz, DMSO)  $\delta_{\text{C}}$  55.61, 109.38, 114.11, 122.52, 124.78, 127.83, 130.08, 133.41, 134.16, 135.31, 146.35, 150.23, 155.94, 156.25, 157.38; IR (KBr)  $\nu_{\text{max}}$ : 829 (s), 1228 (s), 1597 (s), 1642 (s), 3086 (w). MS: Theoretical mass: 390.96 calculated for  $\text{C}_{15}\text{H}_{10}\text{BrN}_3\text{O}_3\text{S}$ ; Found:  $m/z$   $[\text{M}+\text{Na}]^+$ : 413.9.

#### 4.1.4. *N*-(6-methoxy-benzothiazol-2-yl)-4-fluoro-2-nitrobenzylidene amine

(6-Methoxy-benzothiazol-2-yl)-amine **1** (0.54 g, 3 mmol) and 4-fluoro-*o*-nitrobenzaldehyde **2d** (0.51 g, 3 mmol) were reacted to provide the corresponding Schiff base as a reddish solid in 95% yield following purification by column chromatography using DCM as an eluent. M.p. 150–151 °C;  $^1\text{H}$  NMR (300 MHz,  $\text{CDCl}_3$ )  $\delta_{\text{H}}$  3.90 (s, 3H), 7.11 (dd,  $J = 6.25, 3.83$ , 1H), 7.31–7.38 (m, 2H), 7.91 (d,  $J = 3.42$ , 1H), 8.14–8.21 (m, 2H), 9.45 (s, 1H);  $^{13}\text{C}$  NMR (100 MHz,  $\text{CDCl}_3$ )  $\delta_{\text{C}}$  55.83, 104.19, 116.35, 116.55, 116.75, 119.35, 119.54, 125.53, 127.97, 145.99, 158.29, 159.11, 166.07, 167.44; MS: Theoretical mass: 331.04 calculated for  $\text{C}_{15}\text{H}_{10}\text{FN}_3\text{O}_3\text{S}$ ; Found:  $m/z$   $[\text{M}+\text{H}]^+$ : 332.05.

#### 4.1.5. *N*-(6-methoxy-benzothiazol-2-yl)-4-dimethylamino-2-nitrobenzylidene amine

(6-Methoxy-benzothiazol-2-yl)-amine **1** (0.54 g, 3 mmol) and 4-dimethylamino-*o*-nitrobenzaldehyde **2e** (0.58 g, 3 mmol) were used, and the corresponding Schiff base was obtained as a reddish-brown solid in 92% yield. No further purification was required. M.p. 195–197 °C;  $^1\text{H}$  NMR (300 MHz,  $\text{CDCl}_3$ )  $\delta_{\text{H}}$  3.16 (s, 6H), 3.89 (s, 3H), 6.92 (dd,  $J = 8.97, 6.39$ , 1H), 7.07 (dd,  $J = 8.94, 6.36$ , 1H), 7.13–7.30 (m, 2H), 7.85 (d,  $J = 8.91$ , 1H), 8.41 (d,  $J = 9.03$ , 1H), 9.26 (s, 1H);  $^{13}\text{C}$  NMR (100 MHz,  $\text{CDCl}_3$ )  $\delta_{\text{C}}$  40.78, 55.61, 109.38, 112.72, 114.10, 120.09, 124.77, 129.05, 131.66, 134.16, 144.02, 150.22, 153.24, 155.94, 156.22, 157.38; IR (KBr)  $\nu_{\text{max}}$ : 825 (s), 1221 (s), 1619 (s), 2934 (w). MS: Theoretical mass: 331.04 calculated for  $\text{C}_{17}\text{H}_{16}\text{N}_4\text{O}_3\text{S}$ ; Found:  $m/z$   $[\text{M}+\text{H}]^+$ : 332.05.

## 4.2. Synthesis of Benzylamines derivatives

Benzylidene derivatives were pestled and suspended in a minimal amount of methanol, followed by the addition of sodium borohydride (2 equivalents). Effervescence indicated the advancement of the reaction. The reaction proceeded at ambient temperature until TLC showed consumption of the starting material, and a change in color of the crystals occurred. Reduced solids were collected on a Hirsch funnel and washed with cold methanol. No further purification was required.

#### 4.2.1. *N*-(6-methoxy-benzothiazol-2-yl)-2-nitrobenzylamine (**3a**)

The corresponding Schiff base (0.62 g, 2 mmol) was reduced, and provided **3a** as a yellow solid in 95% yield; M.p. 140–143 °C;  $^1\text{H}$  NMR (300 MHz,  $\text{CDCl}_3$ )  $\delta_{\text{H}}$  2.17 (s, 2H), 3.81 (s, 3H), 4.79 (s, 1H), 6.90 (dd,  $J = 6.58, 3.46$ , 1H), 7.10 (d,  $J = 3.48$ , 1H), 7.46 (dd,  $J = 12, 6.56$ , 1H), 7.62 (t,  $J = 9.19$ , 1H), 7.80 (d,  $J = 3.48$ , 1H), 8.11 (d,  $J = 3.81$ , 1H);  $^{13}\text{C}$  NMR (100 MHz,  $\text{CDCl}_3$ )  $\delta_{\text{C}}$  30.94, 46.55, 55.89, 105.46, 113.83, 119.14, 125.36, 128.88, 130.63, 131.28, 133.32, 134.10, 155.59, 165.03, 171.79; IR (KBr)  $\nu_{\text{max}}$ : 821 (s), 1220 (s), 1521 (s), 1625 (s), 2904 (w), 3107 (s); MS: Theoretical mass: 315.07 calculated for  $\text{C}_{15}\text{H}_{13}\text{N}_3\text{O}_3\text{S}$ ; Found:  $m/z$   $[\text{M}+\text{H}]^+$ : 316.08.

#### 4.2.2. *N*-(6-methoxy-benzothiazol-2-yl)-5-chloro-2-nitrobenzylamine (**3b**)

The corresponding benzylidene derivative (0.54 g, 1.5 mmol) was reduced, and **3b** was obtained as a yellow solid in 93% yield. M.p. 138–140 °C;  $^1\text{H}$  NMR (300 MHz, DMSO)  $\delta_{\text{H}}$  3.73 (s, 3H), 4.89 (s, 2H), 6.82 (dd,  $J = 8.73, 6.09$ , 1H), 7.28 (d,  $J = 8.76$ , 1H), 7.34 (d,  $J = 2.58$ , 1H), 7.62–7.65 (m, 2H), 8.12 (d,  $J = 8.43$ , 1H), 8.40 (s, 1H);  $^{13}\text{C}$  NMR (100 MHz, DMSO)  $\delta_{\text{C}}$  41.38, 55.61, 106.55, 113.33, 118.67, 126.68, 127.87, 130.45, 132.89, 135.43, 136.76, 147.47, 154.74, 162.96; IR (neat)  $\nu_{\text{max}}$ : 829 (s), 1340 (s), 1434 (s), 1603 (s), 2901 (w), 3101 (w). MS: Theoretical mass: 349.0 calculated for  $\text{C}_{15}\text{H}_{12}\text{ClN}_3\text{O}_3\text{S}$ ; Found:  $m/z$   $[\text{M}-\text{H}]^-$ : 347.8;

#### 4.2.3. *N*-(6-methoxy-benzothiazol-2-yl)-5-bromo-2-nitrobenzylamine (**3c**)

The corresponding benzylidene adduct (0.5 g, 1.27 mmol) was reduced, and provided **3c** as a yellow solid in 91% yield; M.p. 137–139 °C;  $^1\text{H}$  NMR (300 MHz,  $\text{CDCl}_3$ )  $\delta_{\text{H}}$  3.82 (s, 3H), 4.92 (s, 2H), 6.02 (s, 1H), 6.90 (dd,  $J = 6.21, 2.61$ , 1H), 7.12 (d,  $J = 2.58$ , 1H), 7.42 (d,  $J = 8.82$ , 1H), 7.68–7.75 (m, 1H), 8.22 (s, 1H);  $^{13}\text{C}$  NMR (100 MHz,  $\text{CDCl}_3$ )  $\delta_{\text{C}}$  44.38, 55.61, 106.54, 113.33, 118.67, 121.37, 127.33, 132.16, 132.98, 133.10, 138.45, 146.08, 149.12, 154.73, 162.96; IR (KBr)  $\nu_{\text{max}}$ : 829 (s), 1340 (s), 1473 (s), 1609 (s), 2902 (mb), 3102 (mb). MS: Theoretical mass: 392.97 calculated for  $\text{C}_{15}\text{H}_{12}\text{BrN}_3\text{O}_3\text{S}$ ; Found:  $m/z$   $[\text{M}+\text{H}]^+$ : 393.9.

#### 4.2.4. *N*-(6-methoxy-benzothiazol-2-yl)-4-fluoro-2-nitrobenzylamine (**3d**)

The corresponding Schiff base (0.5 g, 1.5 mmol) was reduced to **3d** which was obtained as a yellow solid in 91% yield; M.p. 140–142 °C;  $^1\text{H}$  NMR (300 MHz,  $\text{CDCl}_3$ )  $\delta_{\text{H}}$  3.80 (s, 3H), 4.98 (s, 2H), 6.88 (dd,  $J = 6.56, 3.04$ , 1H), 7.09–7.11 (m, 2H), 7.41 (d,  $J = 3.51$ , 1H), 7.51 (dd,  $J = 6.59, 3.08$ , 1H), 8.18 (dd,  $J = 6.28, 3.46$ , 1H);  $^{13}\text{C}$  NMR (100 MHz,  $\text{CDCl}_3$ )  $\delta_{\text{C}}$  46.32, 55.83, 105.38, 113.71, 115.52, 115.71, 117.90, 118.09, 119.54, 128.89, 128.37, 131.33, 137.83, 137.90, 144.06, 145.76, 155.52, 164.30, 164.73, 166.35; MS: Theoretical mass: 333.06 calculated for  $\text{C}_{15}\text{H}_{12}\text{FN}_3\text{O}_3\text{S}$ ; Found:  $m/z$   $[\text{M}+\text{H}]^+$ : 334.07.

#### 4.2.5. *N*-(6-methoxy-benzothiazol-2-yl)-4-dimethylamino-2-nitrobenzylamine (**3e**)

The corresponding Schiff base (0.5 g, 1.40 mmol) was reduced, and **3e** was obtained as a red-orange solid in 93% yield; M.p. 162–

164°C;  $^1\text{H}$  NMR (300 MHz,  $\text{CDCl}_3$ )  $\delta_{\text{H}}$  3.16 (s, 6H), 3.89 (s, 3H), 5.30 (s, 2H), 6.92 (dd,  $J = 8.97, 6.39$ , 1H), 7.07 (dd,  $J = 8.94, 6.36$ , 1H), 7.13–7.30 (m, 2H), 7.85 (d,  $J = 8.91$ , 1H), 8.41 (d,  $J = 9.03$ , 1H), 9.26 (s, 1H);  $^{13}\text{C}$  NMR (100 MHz,  $\text{CDCl}_3$ )  $\delta_{\text{C}}$  40.78, 44.38, 55.61, 106.55, 113.33, 115.84, 118.51, 118.67, 129.13, 132.89, 138.41, 142.64, 149.12, 152.78, 154.47, 162.96; IR (KBr)  $\nu_{\text{max}}$ : 826 (s), 1366 (s), 1471 (s), 1599 (s), 2906 (w). MS: Theoretical mass: 358.1 calculated for  $\text{C}_{17}\text{H}_{18}\text{N}_4\text{O}_3\text{S}$ ; Found:  $m/z$  [M-H] $^-$ : 356.7.

### 4.3. Synthesis of Boc-protected linkers

Boc-protected linkers were prepared by the dropwise addition of a diluted solution of di-*tert*-butyl dicarbonate in anhydrous DCM to the corresponding diamine precursor dissolved in DCM in an ice-chilled round bottom flask. The reaction mixture was stirred at room temperature for 18 h after which the volatiles were evaporated. The as-formed residue was extracted dissolved in aqueous  $\text{NaHCO}_3$  and extracted with DCM. The organic aliquot was collected, dried over anhydrous  $\text{MgSO}_4$ , and concentrated *in vacuo*.

#### 4.3.1. $\text{NH}_2$ -EDA-Boc (**8a**)<sup>24</sup>

To a solution of di-*tert*-butyl dicarbonate (1.09 g, 5 mmol) in anhydrous DCM (80 mL) was added a solution of EDA **7a** (1.80 g, 30 mmol) in anhydrous DCM (10 mL). **8a** was obtained as a colorless viscous oil in 94% yield;  $^1\text{H}$  NMR (300 MHz,  $\text{CDCl}_3$ )  $\delta_{\text{H}}$  1.43 (s, 9H), 1.59 (s, 2H), 2.79 (t,  $J = 6.13$ , 2H), 3.16 (d,  $J = 3.35$ , 2H), 4.94 (s, 1H);  $^{13}\text{C}$  NMR (100 MHz,  $\text{CDCl}_3$ )  $\delta_{\text{C}}$  20.38, 41.79, 43.23, 76.7, 77.01, 77.23, 156.21; MS: Theoretical mass: 160.12 calculated for  $\text{C}_7\text{H}_{16}\text{N}_2\text{O}_2$ ; Found:  $m/z$  [M+H] $^+$  162.21.

#### 4.3.2. $\text{NH}_2$ -TEG-Boc (**8b**)<sup>29</sup>

To solution of di-*tert*-butyl dicarbonate (1.09 g, 5 mmol) in anhydrous DCM (80 mL) was added a solution of TEG- $\text{NH}_2$  **7b** (4.44 g, 30 mmol) in anhydrous DCM (10 mL). The desired product **8b** was afforded as a colorless viscous oil in 98% yield;  $^1\text{H}$  NMR (300 MHz,  $\text{CDCl}_3$ )  $\delta_{\text{H}}$  1.43 (s, 9H), 2.80–2.95 (m, 2H), 3.28–3.34 (m, 2H), 3.50–3.65 (m, 10H);  $^{13}\text{C}$  NMR (100 MHz,  $\text{CDCl}_3$ )  $\delta_{\text{C}}$  28.4, 40.31, 41.50, 41.70, 53.26, 70.20, 72.71, 73.35; MS: Theoretical mass: 248.17 calculated for  $\text{C}_{11}\text{H}_{24}\text{N}_2\text{O}_3$ ; Found:  $m/z$  [M+H] $^+$ : 249.18.

### 4.4. Synthesis of the 2H-Indazoles via the Davis-Beirut reaction

Benzylamine derivatives and a linker (EDA, TEG- $\text{NH}_2$ ,  $\text{NH}_2$ -EDA-Boc, or  $\text{NH}_2$ -TEG-Boc) were dissolved in anhydrous THF in a round bottom flask wrapped in aluminum foil. Five drops of DBU were then added, and the reaction mixture was stirred at room temperature for 48 h. The dark solution was concentrated under vacuum and the oily residue was washed with DCM. The obtained precipitate was filtered through a Hirsch funnel and washed with DCM. No further purification was required.

#### 4.4.1. *N*1-(2-(6-methoxybenzo[d]thiazol-2-yl)-2H-indazol-3-yl)ethane-1,2-diamine (**5**)

Benzylamine **3a** (0.3 g; 0.68 mmol) and EDA (0.12 g; 2.04 mmol) were dissolved in THF (10 mL), and provided **5** as a yellow solid in very low yield (<5%); MS: Theoretical mass: 339.12 calculated for  $\text{C}_{15}\text{H}_{13}\text{N}_3\text{O}_3\text{S}$ ; Found:  $m/z$  [M+H] $^+$  340.12.

#### 4.4.2. *N*-(2-(2-(2-Aminoethoxy)ethoxy)ethyl)-2-(6-methoxybenzo[d]thiazol-2-yl)-2H-indazol-3-amine (**6a**)

Benzylamine **3a** (0.3 g; 0.68 mmol) and TEG- $\text{NH}_2$  (0.38 g; 2.04 mmol) were dissolved in THF (10 mL), and provided **6a** as a yellow solid in very low yield (<5%); MS: Theoretical mass: 427.17 calculated for  $\text{C}_{21}\text{H}_{25}\text{N}_5\text{O}_3\text{S}$ ; Found:  $m/z$  [M+H] $^+$  428.17.

#### 4.4.3. *N*-(2-(2-(2-Aminoethoxy)ethoxy)ethyl)-4-fluoro-2-(6-methoxybenzo[d]thiazol-2-yl)-2H-indazol-3-amine (**6d**)

Benzylamine **3d** (0.3 g; 0.89 mmol) and TEG- $\text{NH}_2$  (0.38 g; 2.04 mmol) were dissolved in THF (10 mL), and provided **6d** as a yellow solid in very low yield (<5%); MS: Theoretical mass: 445.16 calculated for  $\text{C}_{21}\text{H}_{24}\text{FN}_5\text{O}_3\text{S}$ ; Found:  $m/z$  [M+H] $^+$  446.12.

#### 4.4.4. *tert*-Butyl(2-((2-(6-methoxybenzo[d]thiazol-2-yl)-2H-indazol-3-yl)amino)ethyl)-carbamate (**9a**)

Benzylamine **3a** (0.3 g, 0.68 mmol) and EDA-Boc **8a** (0.45 g, 2.85 mmol) were reacted, and indazole **9a** was obtained as yellow solid in 38% yield. M.p. 217–219°C;  $^1\text{H}$  NMR (300 MHz,  $\text{CDCl}_3$ )  $\delta_{\text{H}}$  1.43 (s, 9H), 3.55–3.58 (m, 2H), 3.90 (s, 3H), 3.91–3.96 (m, 2H), 5.04 (s, 1H); 6.79 (t,  $J = 6$ , 1H), 7.03–7.08 (m, 1H); 7.32 (d,  $J = 1.8$ , 1H); 7.44 (d,  $J = 6$ , 1H); 7.66 (d,  $J = 6$ , 1H); 7.83 (d,  $J = 15$ , 1H); 8.75 (s, 1H);  $^{13}\text{C}$  NMR (100 MHz,  $\text{CDCl}_3$ )  $\delta_{\text{C}}$  27.23, 28.35, 40.68, 44.69, 55.85, 104.31, 115.56, 116.19, 118.74, 122.30, 122.78, 129.91, 133.63, 144.71, 150.90, 156.08, 157.51; IR (KBr)  $\nu_{\text{max}}$ : 621(m), 1116 (m), 1521 (m), 1676 (s), 3459 (s); MS: Theoretical mass: 439.17 calculated for  $\text{C}_{22}\text{H}_{25}\text{N}_5\text{O}_3\text{S}$ ; Found:  $m/z$  [M+H] $^+$  440.20.

#### 4.4.5. *tert*-Butyl(2-((5-chloro-2-(6-methoxybenzo[d]thiazol-2-yl)-2H-indazol-3-yl)amino)ethyl)carbamate (**9b**)

Benzylamine **3b** (0.3 g, 0.85 mmol) and EDA-Boc **8a** (0.45 g, 2.85 mmol) were used, and **9b** was collected as a yellow solid in 51% yield; M.p. 238–241°C;  $^1\text{H}$  NMR (300 MHz,  $\text{CDCl}_3$ )  $\delta_{\text{H}}$  1.45 (s, 9H), 3.58 (t,  $J = 11.97$ , 2H), 3.88 (t,  $J = 12.45$ , 2H), 3.92 (s, 3H), 7.08–7.14 (m, 2H), 1.34–7.37 (m, 3H), 7.64 (s, 1H), 7.85 (d,  $J = 9.42$ , 1H), 8.54 (t,  $J = 9.72$ , 1H);  $^{13}\text{C}$  NMR (100 MHz,  $\text{CDCl}_3$ )  $\delta_{\text{C}}$  28.30, 40.77, 46.38, 55.61, 79.52, 106.73, 110.65, 113.33, 118.82, 121.43, 121.62, 124.83, 127.77, 133.31, 137.46, 145.78, 149.49, 154.74, 156.81, 158.06; IR (KBr)  $\nu_{\text{max}}$ : 912 (s), 1355 (s), 1470 (s), 1678 (s), 2980 (w). MS: Theoretical mass: 474.1 calculated for  $\text{C}_{22}\text{H}_{24}\text{ClN}_5\text{O}_3\text{S}$ ; Found:  $m/z$  [M+Na] $^+$  497.1.

#### 4.4.6. *tert*-Butyl(2-((5-bromo-2-(6-methoxybenzo[d]thiazol-2-yl)-2H-indazol-3-yl)amino)ethyl)carbamate (**9c**)

Benzylamine **3c** (0.3 g, 0.75 mmol) and EDA-Boc **8a** (0.45 g, 2.85 mmol) were used, and **9c** was collected as a yellow solid in 43% yield; M.p. 224–226°C;  $^1\text{H}$  NMR (300 MHz,  $\text{CDCl}_3$ )  $\delta_{\text{H}}$  1.18 (s, 9H), 3.46 (t,  $J = 12.3$ , 2H), 3.61–3.71 (m, 5H), 4.93 (s, 1H), 6.71 (dd,  $J = 9.09, 7.47$ , 1H), 7 (dd,  $J = 6.36, 2.55$ , 1H), 7.25 (d,  $J = 2.52$ , 1H), 7.49–7.53 (m, 2H), 7.55 (d,  $J = 16.14$ , 1H), 7.47–7.86 (m, 1H);  $^{13}\text{C}$  NMR (100 MHz,  $\text{CDCl}_3$ )  $\delta_{\text{C}}$  28.30, 40.77, 46.83, 55.61, 79.52, 106.73, 111.08, 113.3, 114.83, 118.8, 121, 122.68, 131.25, 133.31, 137.46, 145.08, 149.49, 154.74, 156.81, 158.06. IR (KBr)  $\nu_{\text{max}}$ : 750 (m), 1220 (s), 1498 (m), 1650 (s), 3450 (s); MS: Theoretical mass: 473.6 calculated for  $\text{C}_{22}\text{H}_{24}\text{BrN}_5\text{O}_3\text{S}$ ; Found:  $m/z$  [M+Na] $^+$  497.1.

#### 4.4.7. *tert*-Butyl(2-((4-fluoro-2-(6-methoxybenzo[d]thiazol-2-yl)-2H-indazol-3-yl)amino)ethyl)carbamate (**9d**)

Benzylamine **3d** (0.3 g, 0.65 mmol) and EDA-Boc **8a** (0.45 g, 2.85 mmol) were mixed. Indazole **9d** was afforded as a yellow solid in 62% yield;  $^1\text{H}$  NMR (300 MHz,  $\text{CDCl}_3$ )  $\delta_{\text{H}}$  1.45 (s, 9H), 3.58 (t,  $J = 12.05$ , 2H), 3.85 (m, 5H), 5 (s, 1H), 7.07 (d,  $J = 15.24$ , 1H), 7.35 (dd,  $J = 6.32, 12.34$ , 1H), 7.4 (m, 2H), 7.83 (d,  $J = 12.42$ , 1H), 8.5 (s, 1H);  $^{13}\text{C}$  NMR (100 MHz,  $\text{CDCl}_3$ )  $\delta_{\text{C}}$  28.33, 40.76, 44.69, 55.87, 104.36, 115.63, 117.92, 121.30, 122.83, 133.62, 144.70, 148.42, 154.96, 157.63; MS: Theoretical mass: 457.16 calculated for  $\text{C}_{22}\text{H}_{24}\text{FN}_5\text{O}_3\text{S}$ ; Found:  $m/z$  [M+H] $^+$ : 458.26.

#### 4.4.8. *tert*-Butyl(2-((6-(dimethylamino)-2-(6-methoxybenzo[d]thiazol-2-yl)-2H-indazol-3-yl)amino)ethyl)carbamate (**9e**)

Benzylamine **3e** (0.3 g, 0.65 mmol) and EDA-Boc **8a** (0.45 g, 2.85 mmol) were reacted, and **9e** was obtained as a red-orange

solid in 14% yield; M.p. 171–173 °C;  $^1\text{H}$  NMR (300 MHz,  $\text{CDCl}_3$ )  $\delta_{\text{H}}$  1.61 (s, 6H), 3.02 (s, 9H), 3.82 (s, 3H), 4.78 (s, 2H), 5.94 (s, 1H), 6.90 (d,  $J = 7.98$ , 2H), 7.12 (s, 1H), 7.33 (s, 2H), 7.45 (d,  $J = 8.55$ , 1H), 7.57 (d,  $J = 8.28$ , 1H);  $^{13}\text{C}$  NMR (100 MHz,  $\text{CDCl}_3$ )  $\delta_{\text{C}}$  28.30, 40.78, 46.38, 55.61, 79.52, 106.73, 110.87, 112.84, 113.33, 118.82, 120.17, 122.46, 133.31, 137.46, 138.86, 149, 149.5, 154.74, 156.81, 158.06; IR (KBr)  $\nu_{\text{max}}$ : 833 (s), 1358 (s), 1471 (s), 1607 (s), 2905 (mb), 3105 (mb). MS: Theoretical mass: 482.2 calculated for  $\text{C}_{24}\text{H}_{30}\text{N}_6\text{O}_3\text{S}$ ; Found:  $m/z$  [M-H] $^-$ : 481.0.

#### 4.4.9. tert-Butyl(2-(2-(2-((2-(6-methoxybenzo[d]thiazol-2-yl)-2H-indazol-3-yl)amino)ethoxy)-ethoxy)ethyl)carbamate (**10a**)

Required benzylamine **3a** (0.3 g, 0.68 mmol) and TEG-Boc **8b** (0.66 g, 2.85 mmol), and provided as yellow solid in very low yield (<5%); MS: Theoretical mass: 527.22 calculated for  $\text{C}_{26}\text{H}_{33}\text{N}_5\text{O}_4\text{S}$ ; Found:  $m/z$  [M+H] $^+$  528.22.

#### 4.5. Synthesis of $N^1$ -(2-(2-(2-(6-methoxybenzo[d]thiazol-2-yl)-2H-indazol-3-yl)ethane-1,2-diamine (**11a**))

Indazole **3a** (0.2 g, 0.45 mmol) was dissolved in ice-chilled DCM (10 mL) and TFA (2 mL) was added. The reaction mixture was stirred for 3 h at room temperature after which it was concentrated *in vacuo*. The as-formed yellowish solid was washed with hexane to remove excess TFA. **11a** was obtained as a yellowish solid in 92% yield; M.p. 117–121 °C;  $^1\text{H}$  NMR (300 MHz,  $\text{CDCl}_3$ )  $\delta_{\text{H}}$  3.46 (t,  $J = 12.3$ , 2H), 3.61–3.71 (m, 5H), 4.93 (s, 1H), 6.71 (dd,  $J = 9.09$ , 7.47, 1H), 7 (dd,  $J = 6.36$ , 2.55, 1H), 7.25 (d,  $J = 2.52$ , 1H), 7.49–7.53 (m, 2H), 7.55 (d,  $J = 16.14$ , 1H), 7.47–7.86 (m, 1H);  $^{13}\text{C}$  NMR (100 MHz,  $\text{CDCl}_3$ )  $\delta_{\text{C}}$  28.30, 40.77, 46.83, 55.61, 79.52, 106.73, 111.08, 113.3, 114.83, 118.8, 121, 122.68, 131.25, 133.31, 137.46, 145.08, 149.49, 154.74, 156.81, 158.06. IR (KBr)  $\nu_{\text{max}}$ : 722 (m), 805 (m), 1198 (s), 1540 (m), 1619 (s), 2917 (m), 3443 (s); MS: Theoretical mass: 339.11 calculated for  $\text{C}_{17}\text{H}_{17}\text{N}_5\text{O}_5$ ; Found:  $m/z$  [M+H] $^+$  340.12.

#### 4.6. Synthesis of indazole-loaded nanoparticles

##### 4.6.1. Synthesis of dextran-coated aminated nanoparticles (SPION)

Dextran (4.5 g, 9–11 kDa) was dissolved by sonication in double distilled water (20 mL) and then filtered through 0.22  $\mu\text{m}$  syringe filter.  $\text{FeCl}_3 \cdot 6\text{H}_2\text{O}$  (0.32 g, 1.2 mmol) was added and the mixture was stirred vigorously at 0 °C under nitrogen for 2 h.  $\text{FeCl}_2 \cdot 4\text{H}_2\text{O}$  (0.13 g, 0.65 mmol) in 0.22  $\mu\text{m}$  filtered degassed water (0.9 mL) was then added slowly. Chilled 30%  $\text{NH}_4\text{OH}$  solution (0.9 mL) was added dropwise with rapid stirring resulting in a greenish suspension that was heated at ~85 °C for 90 min. The mixture was then cooled forming black superparamagnetic iron oxide nanoparticles (SPIONs). Ammonium chloride and excess dextran were removed by extensive dialysis (14 kDa cutoff), followed by ultrafiltration (30 kDa cutoff membrane). After several washes, the colloidal product was concentrated by ultrafiltration and filtered through a 0.22  $\mu\text{m}$  membrane filter to a final concentration of 6 mg-NP/mL.

##### 4.6.2. Synthesis of hyaluronan-coated nanoparticles (SPION-HA)

Acetonitrile (2 mL) and NMM (50  $\mu\text{L}$ ) were dropped into HA (70 mg) dissolved in double distilled water (3 mL) by sonication. CDMT (10 mg) was added to the solution of HA and the reaction was allowed to stir at room temperature for 2 h. SPION (2 mL) were then added and the mixture was allowed to at room temperature for 36 h. SPION-HA were purified by ultrafiltration. The hydrodynamic diameter of the nanoparticles was found to be 88.3 nm.

##### 4.6.3. Synthesis of indazole-loaded nanoparticles (SPION-HA-IND)

SPION-HA (2 mL), EDC (0.15 mg; 1 mmol), and NHS (0.46 mg, 4 mmol) were dissolved in MES buffer (10 mL) and the solution was

allowed to stir over 2 h after which time a sonicated solution of indazole **9a** (10 mg, 0.0029 mmol) in MES: DMSO (5:1) was added and the reaction was allowed to stir in the dark at room temperature for 48 h. The nanoparticle solution was diluted with double distilled water and purified by dialysis and centrifugation. The hydrodynamic diameter of the nanoparticles was found to be 139 nm and the polydispersity index was 0.2.

#### 4.6.4. Spectrophotometric analysis

To evaluate the amount of indazole **9a** loaded on the nanoparticles, a standard linear-fit curve of free indazole was created by plotting the UV–Vis absorbance at 230 nm of several indazole standard solutions in methanol. The stock solution was prepared by dissolving 2 mg of **9a** in 10 mL methanol for a concentration of 0.2 mg/mL. The absorbance of standards of serial dilutions of **9a** (0.2; 0.1; 0.05; 0.025; 0.0125 mg/mL) against methanol blank showed a linear correlation between the concentration gradient and the corresponding absorbencies at 230 nm.

The slope gives the value of the molecular absorptivity ( $\epsilon$ ) for indazole **9a** and was calculated to be 12.4. SPION-HA-IND aqueous sample of concentration 0.16 mg/mL was prepared by diluting a 2 mL aliquot of nanoparticle stock solution of initial concentration 0.8 mg/mL to a final volume of 10 mL dd-water. The absorbance at 230 nm was measured against indazole-free SPIONs blank which was prepared by diluting a 266  $\mu\text{L}$  aliquot of SPION-HA aqueous solution of initial concentration 6 mg/mL to a final volume of 10 mL. The concentration of indazole **9a** loaded onto the nanoparticles was then calculated to be: [IND] =  $0.88/12.4 = 0.071$  mg/ml

#### 4.6.5. Determining the $r_2^*$ values for HA-NP

Serial dilutions of the HA-NP were prepared to a final volume of 5 mL in 15 mL-centrifuge tubes (Corning). The tubes were placed on a polystyrene tube holder. All MRI experiments were carried out on a GE 3T Signa<sup>®</sup> HDx MR scanner (GE Healthcare, Waukesha, WI). To evaluate the  $r_2^*$  characteristics of the nanoparticles, the following parameters were used: head coil, 3D fast spoiled gradient recalled (FSPGR) sequence, flip angle = 15°, 16 echo times (TEs) = 2.1 ms, 4.6 ms, 7.0 ms, 9.4 ms, 11.8 ms, 14.3 ms, 16.7 ms, 19.1 ms, 21.5 ms, 24.0 ms, 26.4 ms, 28.8 ms, 31.2 ms, 33.7 ms, 36.1 ms, and 38.5 ms, time of repetition (TR) = 41.9 ms, receiver bandwidth (rBW) =  $\pm 62.5$  kHz, field of view (FOV) = 16 cm, slice thickness = 1.5 mm, number of slices = 16, acquisition matrix = 256  $\times$  256, number of excitation (NEX) = 1, and scan time = 1 min 55 s [Fe] was plotted against (1/T2\*), and  $r_2^*$  is the slope of the generated straight line.

#### Acknowledgments

This work was supported by The National Council for Scientific Research-Lebanon (Grant reference: 01-09-2013). We are grateful for Dr. Walid Saad for running the DLS measurements, and for Dr. David Zhu from Michigan State University for determining magnetic relaxivity.

#### Appendix A. Supplementary data

Supplementary data related to this article can be found at <http://dx.doi.org/10.1016/j.tet.2017.08.027>.

#### References

1. Ali NA, Dar BA, Pradhan V, Farooqui M. *Mini Rev Med Chem.* 2013;13:1792–1800.
2. Thangadurai A, Minu M, Wakode S, Agrawal S, Narasimhan B. *Med Chem Res.* 2012;21:1509–1523.
3. Yuan T, Nahar P, Sharma M, et al. *J Nat Prod.* 2014;77:2316–2320.
4. Blair LM, Sperry J. *J Nat Prod.* 2013;76:794–812.

5. Lee KY, Gowrisankar S, Kim JN. *Tetrahedron Lett.* 2005;46:5387–5391.
6. Hu J, Cheng Y, Yang Y, Rao Y. *Chem Comm.* 2011;47:10133–10135.
7. Fang Y, Wu C, Larock RC, Shi F. *J Org Chem.* 2011;76:8840–8851.
8. Ahn GH, Lee JJ, Jun YM, Lee BM, Kim BH. *Org Biomol Chem.* 2007;5:2472–2485.
9. Song JJ, Yee NK. *Org Lett.* 2000;2:519–521.
10. Sharghi H, Aberi M. *Synlett.* 2014;25:1111–1115.
11. Khatun N, Gogoi A, Basu P, Das P, Patel BK. *RSC Adv.* 2014;4:4080–4084.
12. Conrad WE, Fukazawa R, Haddadin MJ, Kurth MJ. *Org Lett.* 2011;13:3138–3141.
13. Mills AD, Nazer MZ, Haddadin MJ, Kurth MJ. *J Org Chem.* 2006;71:2687–2689.
14. Avila B, Solano DM, Haddadin MJ, Kurth MJ. *Org Lett.* 2011;13:1060–1063.
15. Haddadin MJ, Conrad WE, Kurth MJ. *Mini-Rev Med Chem.* 2012;12:1293–1300.
16. Farber KM, Haddadin MJ, Kurth MJ. *J Org Chem.* 2014;79:6939–6945.
17. Avila B, El-Dakdouki MH, Nazer MZ, et al. *Tetrahedron Lett.* 2012;53:6475–6478.
18. Petros RA, Desimone JM. *Nat Rev Drug Discov.* 2010;9:615–627.
19. Reiss G, Hutten A. *Nat Mater.* 2005;4:725–726.
20. El-Dakdouki MH, El-Boubbou K, Xia J, Kavunja H, Huang X. In: Narain R, ed. *Chemistry of Bioconjugates*. John Wiley & Sons; 2014:281–314.
21. Silva AKA, Espinosa A, Kolosnjaj-Tabi J, Wilhelm C, Gazeau F. In: *Iron Oxides*. Wiley-VCH Verlag GmbH & Co. KGaA; 2016:425–472.
22. Tassa C, Shaw SY, Weissleder R. *Acc Chem Res.* 2011;44:842–852.
23. Wang YX. *Quant Imaging Med Surg.* 2011;1:35–40.
24. Riva E, Comi D, Borrelli S, et al. *Bioorg Med Chem.* 2010;18:8660–8668.
25. El-Dakdouki MH, Xia J, Zhu DC, et al. *ACS Appl Mater Interfaces.* 2014;6:697–705.
26. El-Dakdouki MH, Zhu DC, El-Boubbou K, et al. *Biomacromolecules.* 2012;13:1144–1151.
27. Lapčák L, Lapčák L, De Smedt S, Demeester J, Chabreček P. *Chem Rev.* 1998;98:2663–2684.
28. Abdallah H, Arnaudguilhem C, Abdulrahim H, Lobinski R, Jaber F. *Food Chem.* 2016;192:212–227.
29. Jha S, Ramadori F, Quarta S, et al. *Bioconjug Chem.* 2017;28:222–229.